Self-consistent quasiparticle formulation of a multiphonon method and its application to the neutron-rich ^{20}O nucleus

G. De Gregorio,[1,2] F. Knapp,[3] N. Lo Iudice,[1,2] and P. Vesely[4]
[1]*Dipartimento di Fisica, Università di Napoli Federico II, Napoli, Italy*
[2]*INFN Sezione di Napoli, Napoli, Italy*
[3]*Faculty of Mathematics and Physics, Charles University, Prague, Czech Republic*
[4]*Nuclear Physics Institute, Czech Academy of Sciences, 250 68 Řež, Czech Republic*
(Received 1 February 2016; revised manuscript received 11 March 2016; published 15 April 2016)

A Bogoliubov quasiparticle formulation of an equation-of-motion phonon method, suited for open-shell nuclei, is derived. Like its particle-hole version, it consists of deriving a set of equations of motions whose iterative solution generates an orthonormal basis of n-phonon states ($n = 0,1,2,\ldots$), built of quasiparticle Tamm-Dancoff phonons, which simplifies the solution of the eigenvalue problem. The method is applied to the open-shell neutron-rich ^{20}O for illustrative purposes. A Hartree-Fock-Bogoliubov canonical basis, derived from an intrinsic two-body optimized chiral Hamiltonian, is used to derive and solve the eigenvalue equations in a space encompassing a truncated two-phonon basis. The spurious admixtures induced by the violation of the particle number and the center-of-mass motion are eliminated to a large extent by a Gram-Schmidt orthogonalization procedure. The calculation takes into account the Pauli principle, is self-consistent, and is parameter free except for the energy cutoff used to truncate the two-phonon basis, which induces an increasing depression of the ground state through its strong coupling to the quasiparticle vacuum. Such a cutoff is fixed so as to reproduce the first 1^- level. The two-phonon states are shown to enhance the level density of the low-energy spectrum, consistently with the data, and to induce a fragmentation of the $E1$ strength which, while accounting for the very low $E1$ transitions, is not sufficient to reproduce the experimental cross section in the intermediate energy region. This and other discrepancies suggest the need of including the three-phonon states. These are also expected to offset the action of the two phonons on the quasiparticle vacuum and, therefore, free the calculation from any parameter.

DOI: 10.1103/PhysRevC.93.044314

Fast-growing computer power has enabled the upgrading of traditional many-body methods and the elaboration of new, more advanced, approaches capable of exploring deeply and extensively the properties of stable and exotic nuclei.

Ab initio methods, like no-core shell model (NCSM) [1] and coupled-cluster (CC) theory [2,3], describe with accuracy the bulk and low-lying spectroscopic properties of light nuclei.

More phenomenological approaches are generally needed as one moves to heavy regions. Large-scale shell-model calculations based on the Lanczos algorithm [4] or Monte Carlo sampling [5] have provided complete and systematic descriptions of low-energy spectroscopy in medium and heavy nuclei, including those away from the stability line [6,7]. An importance sampling shell model [8] has investigated the spectra of a chain of isotopes and isotones around ^{132}Sn [9–11].

Mean field approaches, like random phase approximation (RPA), are suited for low- and high-energy spectra. They are usually based on Skyrme or relativistic energy density functionals or Gogny forces [12].

Several RPA extensions are now available that allow one to study the fragmentation of the giant resonances and, in general, the fine structure of collective soft modes.

Widely adopted are the RPA plus particle-vibration coupling (PVC) [13], where single-nucleon states couple to collective low-lying nuclear vibrations or phonons, and the quasiparticle phonon model (QPM) [14], which uses a separable Hamiltonian in a multiphonon space covering up to a fraction of three RPA phonons.

Other methods have been proposed in recent years. The relativistic quasiparticle time blocking approximation (RTBA), framed within a covariant energy density functional theory, couples two-quasiparticle states to collective vibrations [15,16]. Two-particle–two-hole configurations are explicitly included in self-consistent second RPA (SRPA) calculations, employing realistic interactions derived by means of the unitary correlation operator method (UCOM) [17] or Skyrme forces [18].

Most RPA extensions, like the RPA plus PVC [19] or RTBA [15,20,21] or QPM [22,23], were adopted to investigate the nature of the low-lying dipole peaks, just below the giant dipole resonance (GDR), presumed to be a manifestation of a soft mode arising from a translational oscillation of the neutron skin against a $N = Z$ core [24] and known as pygmy dipole resonance (PDR).

Low-lying dipole excitations were observed in neutron-rich oxygen isotopes [25–27] and, since then, in several other regions [28–34]. A fairly complete list of experimental and theoretical works can be found in the reviews [20,35,36].

We have proposed an equation-of-motion phonon method (EMPM) [37–39] that derives and solves iteratively a set of equations of motion to generate an orthonormal basis of multiphonon states built of phonons obtained in Tamm-Dancoff approximation (TDA). Such a basis simplifies the structure of the Hamiltonian matrix and makes feasible its diagonalization in large configuration and phonon spaces. The diagonalization produces at once the totality of eigenstates allowed by the dimensions of the multiphonon space. The formalism treats one-phonon as well as multiphonon states on the same footing, takes into account the Pauli principle, and holds for any Hamiltonian.

The method was formulated in the particle-hole (p-h) scheme and first applied to ^{16}O by diagonalizing a realistic Hamiltonian in a space encompassing a fraction of three-phonon states [39]. The coupling of these configurations shifted downward the one-phonon energies toward the restoration of the correct separation of the centroid of the GDR from the correlated ground state, strongly depressed by the coupling of the HF vacuum to the two-phonon subspace.

It was, then, adopted to investigate the dipole response in the heavy, neutron-rich, ^{208}Pb [40,41] and ^{132}Sn [42]. The most recent calculations [41,42] were fully self-consistent and included up to two-phonon basis states, which enhanced greatly the fragmentation of the GDR and the density of low-lying levels associated to the PDR.

Here we derive a quasiparticle version of the method so as to allow the study of open-shell nuclei. After presenting in Sec. I a quasiparticle Hamiltonian in the Hartree-Fock-Bogoliubov (HFB) canonical basis and constructing the TDA phonons in Sec. II, we outline in Sec. III the method by showing how the multiphonon basis is generated and then used to solve the eigenvalue problem. It will emerge clearly that the quasiparticle formulation keeps the simplicity and transparency of the p-h scheme.

The numerical implementation of the method is outlined in Sec. IV. ^{20}O, as representative of neutron-rich oxygen isotopes, is chosen as a testing ground for the method. This is one of the best-studied oxygen isotopes away from the stability line [20,35]. It displays a fairly rich low-lying spectrum [43–46] and exhibits a dipole strength distribution over a rather large energy range [25–27,47].

The low-lying spectra of ^{20}O and other oxygen and carbon neutron-rich isotopes were calculated using the CC theory [48]. Oxygen isotopes were further studied within the same CC approach [49,50] and in an extended $(sdf_{7/2}p_{3/2})$ shell-model valence space using an effective potential which includes chiral two- and three-body interactions up to third order [48–51]. The low-lying 2^+ was also the object of a QRPA study based on Skyrme forces [52].

The dipole strength distribution was investigated within a phenomenological shell-model context [53], relativistic RPA [54], time-dependent HF (TDHF) [55,56], and RPA plus PVC [19]. The objective of these studies was to establish if the low-lying peaks are a manifestation of the PDR or are simply single-particle excitations.

We adopt our method to calculate the full spectrum as well as the dipole strength distribution. We use the chiral potential $V_\chi = \mathrm{NNLO_{opt}}$, optimized so as to minimize the three-body contribution [57], and construct and solve the eigenvalue equations in a space covering up to two-phonon states.

I. THE QUASIPARTICLE HAMILTONIAN IN THE HFB CANONICAL BASIS

A. The starting intrinsic Hamiltonian

The Hamiltonian is composed of an intrinsic kinetic term $T_{\rm int}$ and a nucleon-nucleon (NN) potential V_{NN}. It can be written in the more standard form,

$$H = T + V = T + V_{NN} + T_2, \tag{1}$$

where

$$T = \left(1 - \frac{1}{A}\right)\frac{1}{2m}\sum_i p_i^2 \tag{2}$$

is a modified one-body kinetic term and

$$T_2 = -\frac{1}{2mA}\sum_{i\neq j}\vec{p}_i\cdot\vec{p}_j \tag{3}$$

is a two-body kinetic piece. The second quantized form of T is

$$T = \sum_r [r]^{1/2} t_{rs}(a_r^\dagger \times b_s)^0, \tag{4}$$

where $a_r^\dagger = a^\dagger_{x_r j_r m_r}$ and $b_r = (-)^{j_r+m_r} a_{x_r j_r -m_r}$ are particle creation and annihilation operators, respectively. We have put $[r] = 2j_r + 1$ and use this notation throughout the paper. We also use the symbol $\times$ to denote coupling of two tensor operators to angular momentum Ω.

For V we have

$$V = -\frac{1}{4}\sum_{rstq\Omega}[\Omega]^{1/2} V^\Omega_{rstq}[(a_r^\dagger \times a_s^\dagger)^\Omega \times (b_t \times b_q)^\Omega]^0, \tag{5}$$

where

$$\begin{aligned} V^\Omega_{rstq} &= \langle (t\times q)^\Omega | V | (r\times s)^\Omega\rangle \\ &\quad - (-)^{r+s-\Omega}\langle (t\times q)^\Omega | V | (s\times r)^\Omega\rangle \end{aligned} \tag{6}$$

is un-normalized and antisymmetrized.

B. The quasiparticle Hamiltonian

In the HFB canonical basis, the quasiparticle operators have the BCS form,

$$\begin{aligned} \alpha_r^\dagger &= u_r a_r^\dagger + v_r b_r, \\ \beta_r &= u_r b_r - v_r a_r^\dagger, \end{aligned} \tag{7}$$

where

$$\beta_r = (-)^{j_r+m_r}\alpha_{j_r-m_r}. \tag{8}$$

In its normal form with respect to the HFB vacuum, the Hamiltonian becomes

$$H = E_0 + H_{11} + \mathcal{V}, \tag{9}$$

where E_0 is the HFB ground-state energy, H_{11} is a one-body quasiparticle Hamiltonian, and $\mathcal{V}$ is a two-body potential describing the interaction among quasiparticles. The one-body piece in the angular momentum coupled scheme has the expression

$$H_{11} = \sum_{rs}[r]^{1/2}\mathcal{E}_{rs}[\alpha_r^\dagger \times \beta_s]^0, \tag{10}$$

where

$$\mathcal{E}_{rs} = (\epsilon_{rs} - \lambda\delta_{rs})(u_r u_s - v_r v_s) + \Delta_{rs}(u_r v_s + v_r u_s). \tag{11}$$

Here

$$\epsilon_{rs} = t_{rs} + \Gamma_{rs} \tag{12}$$

and

$$\Gamma_{rs} = \frac{1}{[r]^{1/2}} \sum_t [t]^{1/2} F^0_{rstt} v_t^2, \tag{13}$$

$$\Delta_{rs} = \frac{1}{2} \frac{1}{[r]^{1/2}} \sum_t [t]^{1/2} V^0_{rstt} u_t v_t, \tag{14}$$

are the Hartree-Fock and pairing potentials, respectively. We have introduced the quantity

$$F^\sigma_{rtsq} = \sum_\Omega (-)^{r+q-\sigma-\Omega} [\Omega] W(rstq; \Omega\sigma) V^\Omega_{rstq}, \tag{15}$$

where W is a Racah coefficient. It is to be pointed out that the one-body quasiparticle Hamiltonian does not have the standard diagonal structure, as would have been the case had we used the full HFB basis.

The transformed two-body piece has the composite form,

$$\mathcal{V}_2 = V_{22} + V_{31} + V_{40} + V_{13} + V_{04}, \tag{16}$$

where V_{ij} are expressed in terms of products of i creation and j annihilation quasiparticle operators and V_{ji} are the Hermitian conjugate of V_{ij}. The explicit expressions of V_{ij} are

$$V_{22} = -\sum_{r\leqslant s\, t\leqslant q}^{\sigma} [\sigma]^{1/2} \zeta_{rs}^2 \zeta_{tq}^2 V^\sigma_{rstq}(22) \times [(\alpha_r^\dagger \times \alpha_s^\dagger)^\sigma \times (\beta_t \times \beta_q)^\sigma]^0, \tag{17}$$

$$V_{31} = \frac{1}{2} \sum_{(r\leqslant s)tq}^{\sigma} [\sigma]^{1/2} \zeta_{rs}^2 V^\sigma_{rstq}(31) \times [(\alpha_r^\dagger \times \alpha_s^\dagger)^\sigma \times (\alpha_t^\dagger \times \beta_q)^\sigma]^0, \tag{18}$$

$$V_{40} = \sum_{r\leqslant s\, t\leqslant q}^{\sigma} [\sigma]^{1/2} \zeta_{rs}^2 \zeta_{tq}^2 V^\sigma_{rstq}(40) \times [(\alpha_r^\dagger \times \alpha_s^\dagger)^\Omega \times (\alpha_t^\dagger \times \alpha_q^\dagger)^\sigma]^0, \tag{19}$$

where $\zeta_{rs} = (1+\delta_{rs})^{-1/2}$ and

$$V^\sigma_{rstq}(22) = \big[V^\sigma_{rstq}(u_r u_s u_t u_q + v_r v_s v_t v_q) + F^\sigma_{rstq}(u_r v_s v_t u_q + u_s v_r v_q u_t) + (-)^{r-s-\sigma} F^\sigma_{srtq}(u_s v_r v_t u_q + u_r v_s u_t v_q)\big], \tag{20}$$

$$V^\sigma_{rstq}(31) = \big[F^\sigma_{rstq}(u_r v_s u_t u_q - u_s v_r v_t v_q) - (-)^{r+s-\sigma} F^\sigma_{rsqt}(u_s v_r u_t u_q - u_r v_s v_t v_q)\big], \tag{21}$$

$$V^\sigma_{rstq}(40) = \big[F^\sigma_{rstq}(u_r v_s u_t v_q + u_s v_r v_t u_q) - (-)^{r+s-\sigma} F^\sigma_{rsqt}(u_r v_s v_t u_q + u_s v_r u_t v_q)\big]. \tag{22}$$

II. SELF-CONSISTENT QUASIPARTICLE TAMM-DANCOFF

The TDA consists of solving the eigenvalue equation

$$\langle 0|\big[\overline{Z}^\lambda_{rs}, H\big]^\lambda|\lambda\rangle = \omega_\lambda c^\lambda_{rs} = (E_\lambda - E_0) c^\lambda_{rs}, \tag{23}$$

where

$$c^\lambda_{rs} = \langle (r\times s)^\lambda|\lambda\rangle = \langle 0|\overline{Z}^\lambda_{rs}|\lambda\rangle \tag{24}$$

and $\overline{Z}^\lambda_{rs}$ $(r\leqslant s)$ is the adjoint of the normalized two-quasiparticle operator,

$$Z^\lambda_{rs} = -\zeta_{rs}(\alpha_r^\dagger \times \alpha_s^\dagger)^\lambda. \tag{25}$$

Upon expansion of the commutator, we obtain

$$\sum_{t\leqslant q} A^\lambda_{rstq} c^\lambda_{tq} = (E_\lambda - E_0) c^\lambda_{rs}, \tag{26}$$

where

$$A^\lambda_{rstq} = \zeta_{rs}\zeta_{tq}\big[H_{rstq}(11) + \mathcal{V}^\lambda_{rstq}(22)\big]. \tag{27}$$

The first piece is

$$H_{rstq}(11) = \delta_{sq}\mathcal{E}_{rt} + \delta_{rt}\mathcal{E}_{sq} - (-)^{r+s-\lambda}[\delta_{st}\mathcal{E}_{rq} + \delta_{rq}\mathcal{E}_{st}]. \tag{28}$$

It is to be noted that the above matrix element is nondiagonal as would be the case if computed in the full HFB basis. The second term is the two-body matrix element (20).

The solution of the eigenvalue equation yields the TDA eigenvalues and eigenvectors of the form

$$|\lambda\rangle = O^\dagger_\lambda|0\rangle, \tag{29}$$

where

$$O^\dagger_\lambda = \sum_{r\leqslant s} c^\lambda_{rs} Z^\lambda_{rs} \tag{30}$$

is the TDA phonon operator.

The TDA wave functions can be used to compute the density matrix

$$\rho_{\lambda\lambda'}([r\times s]^\sigma) = \langle\lambda'||(\alpha_r^\dagger \times \beta_s)^\sigma||\lambda\rangle = [\lambda\lambda'\sigma]^{1/2} \sum_t \zeta_{ts}\zeta_{tr}\big[c^\lambda_{t\leqslant s} + (-)^{t-s-\lambda} c^\lambda_{s\leqslant t}\big] \times \big[c^{\lambda'}_{t\leqslant r} + (-)^{r-t-\lambda'} c^{\lambda'}_{r\leqslant t}\big] W(\lambda' t\sigma s; r\lambda). \tag{31}$$

This quantity plays a crucial role in the method. Of equal importance are the amplitudes of the transitions from the ground state induced by a multipole operator,

$$\mathcal{M}(\lambda) = \frac{1}{[\lambda]^{1/2}} \sum_{rs} \langle r||\mathcal{M}(\lambda)||s\rangle [a_r^\dagger \times b_s]^\lambda. \tag{32}$$

After expressing the above operator in terms of quasiparticles, we get the TDA transition matrix elements

$$\langle x\lambda||\mathcal{M}_\lambda||0\rangle = \sum_{r\leqslant s} \langle r||\mathcal{M}_\lambda||s\rangle \zeta_{rs}[u_r v_s + (-)^\lambda u_s v_r] c^\lambda_{rs}(x). \tag{33}$$

Here we need to introduce explicitly the additional quantum number x to label the different TDA states of spin J_λ. We use, otherwise, λ to denote all TDA quantum numbers.

1. Removal of spurious admixtures

For the $J^\pi = 1^-$ and $J^\pi = 0^+$, we need to remove the spurious contamination induced by the center-of-mass (c.m.) motion and by the violation of the number of particles.

Determining the exact form of spurious states is not obvious. The c.m. spurious state, for instance, is easily derived for a harmonic oscillator (HO) external potential. This is not the case for an intrinsic Hamiltonian using a HF (HFB) potential. Thus, as proposed in Ref. [58], we eliminate the spurious admixtures by constructing a basis in the two-quasiparticle space which does not couple to the HF vacuum through the c.m. coordinate and the number operator.

To this purpose we construct for the c.m. the state

$$|\lambda_1\rangle = \frac{1}{N_1} R_\mu |0\rangle = \frac{1}{N_1} \sum_{r\leqslant s} c_{rs}^{\lambda_1} |(r\times s)^{1^-}\rangle, \tag{34}$$

where R_μ is the c.m. coordinate, $c_{rs}^{\lambda_1}$ are the un-normalized coefficients,

$$c_{rs}^{\lambda_1} = \sqrt{\frac{4\pi}{9}} \frac{1}{A} \langle r||rY_1||s\rangle (u_r v_s - u_s v_r), \tag{35}$$

and N_1 is the normalization constant,

$$N_1^2 = \sum_{r\leqslant s} \left|c_{rs}^{\lambda_1}\right|^2. \tag{36}$$

Similarly, we determine for the particle number operator the state

$$|\lambda_0\rangle = \frac{1}{N_0} \sum_{r} c_{rr}^{\lambda_0} |(r\times s)^{0^+}\rangle, \tag{37}$$

where $c_{rr}^{\lambda_0}$ are the un-normalized coefficients,

$$c_{rr}^{\lambda_0} = \sqrt{2[r]} (u_r v_r), \tag{38}$$

and N_0 is the normalization factor,

$$N_0^2 = \sum_{r} \left|c_{rr}^{\lambda_0}\right|^2. \tag{39}$$

We then apply the Gramm-Schmidt orthogonalization procedure to the $J^\pi = 1^-$ and $J^\pi = 0^+$ two-quasiparticle states and determine the basis states $|\Phi_i\rangle$ orthogonal to $|\lambda_1\rangle$ and $|\lambda_0\rangle$, respectively. The states $|\Phi_i\rangle$, which are linear combinations of the two-quasiparticle states $|(r\times s)^\lambda\rangle$ ($\lambda = 0^+$ or $\lambda = 1^-$), must be used to construct and diagonalize the Hamiltonian matrix, yielding eigenstates rigorously free of spurious admixtures. These eigenstates recover the standard TDA structure given by Eq. (30) once the states $|\Phi_i\rangle$ are expressed in terms of the original two-quasiparticle configurations $|(r\times s)^\lambda\rangle$.

III. EQUATION-OF-MOTION PHONON METHOD

A. Derivation of the *n*-phonon basis

The primary objective of the method is to generate an orthonormal basis of n-phonon states ($n = 1,2,\ldots$) of the form

$$|n;\beta\rangle = \sum_{\lambda\alpha} C_{\lambda\alpha}^\beta |(\lambda\times\alpha)^\beta\rangle = \sum_{\lambda\alpha} C_{\lambda\alpha}^\beta \{O_\lambda^\dagger \times |n-1,\alpha\rangle\}^\beta, \tag{40}$$

where the TDA phonon operator $O_\lambda^\dagger$ (30), of energy E_λ, acts on a $(n-1)$-phonon state $|n-1,\alpha\rangle$, of energy E_α, assumed to be known.

The key for generating such a basis is provided by the equations of motion,

$$\langle n,\beta|\{[H,O_\lambda^\dagger]\times|n-1,\alpha\rangle\}^\beta = (E_\beta - E_\alpha)\langle n,\beta|\{O_\lambda^\dagger\times|n-1,\alpha\rangle\}^\beta. \tag{41}$$

Upon applying the Wigner-Eckart theorem, we obtain the equivalent equations

$$\langle n,\beta||[H,O_\lambda^\dagger]||n-1,\alpha\rangle = (E_\beta - E_\alpha)\langle n,\beta||O_\lambda^\dagger||n-1,\alpha\rangle. \tag{42}$$

We then expand the commutator and invert Eq. (30) to express the two-quasiparticle operators, appearing in the expanded commutator, in terms of the phonon operators $O_\lambda^\dagger$. The outcome of this action is [39]

$$\sum_{\lambda'\alpha'} \mathcal{A}_{\lambda\alpha\lambda'\alpha'}^\beta X_{\lambda'\alpha'}^\beta = E_\beta X_{\lambda\alpha}^\beta, \tag{43}$$

where X defines the amplitude

$$X_{\lambda\alpha}^\beta = \langle n,\beta||O_\lambda^\dagger||n-1,\alpha\rangle \tag{44}$$

and $\mathcal{A}$ is a matrix of the simple structure

$$\mathcal{A}_{\lambda\alpha\lambda'\alpha'}^\beta = (E_\lambda + E_\alpha)\delta_{\lambda\lambda'}\delta_{\alpha\alpha'} + \sum_\sigma W(\beta\lambda'\alpha\sigma;\alpha'\lambda)\mathcal{V}_{\lambda\alpha\lambda'\alpha'}^\sigma. \tag{45}$$

The potential in $\mathcal{A}$ is

$$\mathcal{V}_{\lambda\alpha\lambda'\alpha'}^\sigma = \frac{1}{2}\sum_{rtsq} \rho_{\lambda\lambda'}([r\times t]^\sigma)\mathcal{V}_{rtsq}^\sigma(22)\rho_{\alpha\alpha'}^{(n-1)}([s\times q]^\sigma), \tag{46}$$

where $\rho_{\alpha\alpha'}^{(n)}([r\times s]^\sigma)$ is the n-phonon density matrix,

$$\rho_{\alpha\alpha'}^{(n)}([r\times s]^\sigma) = \langle n;\alpha'||[\alpha_r^\dagger\times\beta_s]^\sigma||n;\alpha\rangle = [\alpha]^{1/2}\Bigg\{\sum_{\lambda\lambda'\gamma}\rho_{\lambda\lambda'}([r\times s]^\sigma)W(\alpha'\sigma\gamma\lambda;\alpha\lambda') \times C_{\lambda\gamma}^{(\alpha)}(n)\,X_{\lambda'\gamma}^{(\alpha')}(n) + \sum_{\gamma\gamma'\lambda}\rho_{\gamma\gamma'}^{(n-1)}([r\times s]^\sigma) \times W(\alpha\sigma\lambda\gamma';\alpha'\gamma)C_{\lambda\gamma}^{(\alpha)}(n)\,X_{\lambda\gamma'}^{(\alpha')}(n)\Bigg\}. \tag{47}$$

The potential accounts for the interaction between one and $(n-1)$ phonons. For $n = 2$ it is simply a phonon-phonon potential.

The formal analogy between the structure of the phonon matrix $\mathcal{A}_{\lambda\alpha\lambda'\alpha'}^\beta$ [Eq. (45)] and the form of the TDA matrix A_{rstq}^λ [Eq. (27)] has been analyzed in detail [39]. The first is deduced from the second by replacing the quasiparticle one-body term with the phonon energies and the interaction among quasiparticles with the interaction among phonons.

Equation (43) is not an eigenvalue equation yet. We have first to expand the amplitudes X [Eq. (44)] in terms of the expansion coefficients $C^{\beta}_{\lambda\alpha}$ of the states $|n;\beta\rangle$ [Eq. (40)] obtaining

$$X^{\beta}_{\lambda\alpha} = \sum_{\lambda'\alpha'} \mathcal{D}^{\beta}_{\lambda\alpha\lambda'\alpha'} C^{\beta}_{\lambda'\alpha'}, \tag{48}$$

where $\mathcal{D}$ is the metric or overlap matrix given by

$$\begin{aligned}\mathcal{D}^{\beta}_{\lambda\alpha\lambda'\alpha'} &= \langle(\lambda\times\alpha)^{\beta}|(\lambda'\times\alpha')^{\beta}\rangle \\ &= \delta_{\lambda\lambda'}\delta_{\alpha\alpha'} - (-)^{\alpha+\beta+\lambda}\sum_{\sigma} W(\lambda'\lambda\alpha'\alpha;\sigma\beta) \\ &\quad\times \sum_{rs}\rho_{\lambda\lambda'}([r\times s]^{\sigma})\rho^{(n-1)}_{\alpha'\alpha}([r\times s]^{\sigma}) \\ &\quad + \sum_{\gamma} W(\alpha'\lambda\lambda'\alpha;\gamma\beta)X^{\alpha}_{\lambda'\gamma}(n-1)X^{\alpha'}_{\lambda\gamma}(n-1),\end{aligned} \tag{49}$$

and $X^{\alpha}_{\lambda\gamma}(n-1) = \langle n-1,\alpha||O^{\dagger}_{\lambda}||n-2,\gamma\rangle$. The above formula shows that the overlap matrix $\mathcal{D}$ reestablishes the Pauli principle by reintroducing the exchange terms among different phonons, in addition to the Kronecker product.

Upon insertion of the expansion (48) into Eq. (43), we get

$$\begin{aligned}\sum_{\lambda'\alpha'}\mathcal{H}^{\beta}_{\lambda\alpha\lambda'\alpha'}C^{\beta}_{\lambda'\alpha'} &= \sum_{\lambda'\alpha'}(A\mathcal{D}^{\beta}_{\lambda\alpha\lambda'\alpha'})C^{\beta}_{\lambda'\alpha'} \\ &= E_{\beta}\sum_{\lambda'\alpha'}\mathcal{D}^{\beta}_{\lambda\alpha\lambda'\alpha'}C^{\beta}_{\lambda'\alpha'}.\end{aligned} \tag{50}$$

These represent the generalized eigenvalue equation

$$\mathcal{H}C = (\mathcal{A}\mathcal{D})C = EC \tag{51}$$

in the states $|(\lambda\times\alpha)^{\beta}\rangle = \{O^{\dagger}_{\lambda}\times|n-1,\alpha\rangle\}^{\beta}$, which form an overcomplete basis.

We eliminate such a redundancy by following the procedure outlined in Refs. [37,38], based on the Cholesky decomposition method. This method selects a basis of linear independent states $|(\lambda\times\alpha)^{\beta}\rangle$ spanning the physical subspace of the correct dimensions $N_n < N_r$ and, thus, enables us to construct a $N_n\times N_n$ nonsingular matrix $\mathcal{D}_n$. By left multiplication in the N_n-dimensional subspace we get from Eq. (51)

$$\left[\mathcal{D}_n^{-1}\mathcal{H}\right]C = \left[\mathcal{D}_n^{-1}(\mathcal{A}\mathcal{D})\right]C = EC. \tag{52}$$

This equation determines only the coefficients $C^{\beta}_{\lambda\alpha}$ of the N_n-dimensional physical subspace. The remaining redundant $N_r - N_n$ coefficients are undetermined and, therefore, can be safely put equal to zero.

The eigenvalue problem within the n-phonon subspace is thereby solved exactly and yields a basis of orthonormal correlated n-phonon states of the form (40).

Because recursive formulas hold for all quantities entering $\mathcal{A}$ and $\mathcal{D}$, it is possible to solve the eigenvalue equations iteratively starting from the TDA phonons and, thereby, generate a set of orthonormal multiphonon states for any n.

B. Eigenvalue problem in the multiphonon basis

We are now ready to formulate the eigenvalue problem in the full space spanned by $\{|0\rangle,|n=1;\alpha_1\rangle,|n=2;\alpha_2\rangle,\ldots,|n,\alpha_n\rangle,\ldots\}$. In such a basis, the eigenvalue equations become

$$\sum_{n'\beta_{n'}}\left[\left(E_{\alpha_n}-\mathcal{E}_{\nu}\right)\delta_{nn'}\delta_{\alpha_n\beta_{n'}} + \mathcal{V}_{\alpha_n\beta_{n'}}\right]\mathcal{C}^{(\nu)}_{\beta_{n'}} = 0, \tag{53}$$

where we used the simpler notation $\alpha_n = (n\alpha)$. The potential has the structure

$$\mathcal{V}_{\alpha_n\beta_{n'}} = \delta_{n'(n-1)}\mathcal{V}^{(31)}_{\alpha\beta} + \delta_{n'(n-2)}\mathcal{V}^{(40)}_{\alpha\beta}. \tag{54}$$

The matrix elements of $\mathcal{V}^{(31)}$ are

$$\mathcal{V}^{(31)}_{\alpha_n\beta_{n'}} = [\alpha]^{-1}\sum_{\sigma\gamma}(-)^{\alpha+\gamma+\sigma}\mathcal{V}^{\sigma}_{\beta\gamma}X^{(\alpha)}_{\sigma\gamma}, \tag{55}$$

where

$$\mathcal{V}^{\sigma}_{\beta\gamma} = \sum_{tq}\mathcal{V}^{\sigma}_{tq}\rho^{(n')}_{\beta\gamma}([t\times q]^{\sigma}) \tag{56}$$

and

$$\begin{aligned}\mathcal{V}^{\sigma}_{tq} = \frac{1}{2}\sum_{r\leqslant s} c^{\sigma}_{rs}\zeta_{rs}\big[&F^{\sigma}_{rstq}(u_r v_s u_t u_q - v_r u_s v_t v_q) \\ &+(-)^{t-q-\sigma}F^{\sigma}_{rsqt}(u_s v_r u_t u_q - v_s u_r v_t v_q)\big].\end{aligned} \tag{57}$$

For $\mathcal{V}^{(40)}_{\alpha\beta}$ we have

$$\mathcal{V}^{(40)}_{\alpha_n\beta_{n'}} = [\alpha]^{-1}\sum_{xy\sigma\gamma}(-)^{\alpha+\gamma+\sigma}X^{\alpha}_{(x\sigma)\gamma}X^{\gamma}_{(y\sigma)\beta}\mathcal{V}^{(\sigma)}_{xy}, \tag{58}$$

where

$$\begin{aligned}\mathcal{V}^{(\sigma)}_{xy} = \frac{1}{4}\sum_{(r\leqslant s)(t\leqslant q)}&\zeta_{rs}\zeta_{tq}c^{\sigma}_{rs}(x)c^{\sigma}_{tq}(y) \\ &\times\big[F^{\sigma}_{rstq}(u_r v_s u_t v_q + u_s v_r u_q v_t) \\ &+(-)^{r-s-\sigma}F^{\sigma}_{srtq}(u_s v_r u_t v_q + u_r v_s u_q v_t)\big].\end{aligned} \tag{59}$$

The solution of the full eigenvalue equations (53) yields the final eigenvalues $\mathcal{E}_{\nu}$ and the corresponding eigenfunctions

$$|\Psi_{\nu}\rangle = \sum_{\alpha_n}\mathcal{C}^{(\nu)}_{\alpha_n}|\alpha_n\rangle, \tag{60}$$

where $|\alpha_n\rangle$ form a basis of orthonormal n-phonon states of the structure given by Eq. (40), namely,

$$|\alpha_n\rangle = \sum_{\lambda\alpha_{(n-1)}} C^{(\alpha_n)}_{\lambda\alpha_{(n-1)}}|(\lambda\times\alpha_{(n-1)})^{\alpha_n}\rangle. \tag{61}$$

The above eigenfunctions, including the ground state, are highly correlated and are the outcome of a procedure which does not rely on any approximation, except for the ones inherent in the HFB transformation and the truncation of the configuration and phonon spaces.

C. Transition amplitudes

For a one-body λ-multipole operator of the form (32) the amplitudes of the transition from initial $|i\rangle$ to final $|f\rangle$ states

of the EMPM form (60) are

$$\langle f||\mathcal{M}(\lambda)||i\rangle = \sum_{n\alpha_{n-1}\beta_n}\Bigg[\mathcal{C}^{(f)}_{\beta_n}\mathcal{C}^{(i)}_{\alpha_{n-1}}\langle\beta_n||\mathcal{M}(\lambda)||\alpha_{n-1}\rangle + (-)^{f-i}\sum_{n\alpha_n\beta_{n-1}}\mathcal{C}^{(i)}_{\alpha_n}\mathcal{C}^{(f)}_{\beta_{n-1}}\langle\alpha_n||\mathcal{M}(\lambda)||\beta_{n-1}\rangle + \sum_{n\alpha_n\beta_n}\mathcal{C}^{(i)}_{\alpha_n}\mathcal{C}^{(f)}_{\beta_n}\langle\beta_n||\mathcal{M}(\lambda)||\alpha_n\rangle\Bigg], \quad (62)$$

where

$$\langle\beta_n||\mathcal{M}(\lambda)||\alpha_{(n-1)}\rangle = \frac{1}{[\lambda]^{1/2}}\sum_x\langle x\lambda||\mathcal{M}(\lambda)||0^+\rangle X^{(\beta_n)}_{(x\lambda)\alpha_{n-1}}, \quad (63)$$

$$\langle\alpha_n||\mathcal{M}(\lambda)||\beta_{n-1}\rangle = \frac{1}{[\lambda]^{1/2}}\sum_x\langle x\lambda||\mathcal{M}(\lambda)||0^+\rangle X^{\alpha_n}_{(x\lambda)\beta_{n-1}}, \quad (64)$$

$$\langle\beta_n||\mathcal{M}(\lambda)||\alpha_n\rangle = \frac{1}{[\lambda]^{1/2}}\sum_{rs}\mathcal{M}^{(-)}_{rs}(\lambda)\rho_{\alpha_n\beta_n}([r\times s]^\lambda). \quad (65)$$

The matrix elements (63) and (64) couple states differing by one phonon and are determined by the TDA transition amplitude $\langle x\lambda||\mathcal{M}(\lambda)||0^+\rangle$ [Eq. (33)] and the amplitudes

$$X^{\beta_n}_{(x\lambda)\alpha_{n-1}} = \langle n\beta, J_f||O^\dagger_{x\lambda}||(n-1),\alpha,J_i\rangle, \quad (66)$$

$$X^{\alpha_n}_{(x\lambda)\beta_{n-1}} = \langle n,\alpha,J_i||O^\dagger_{x\lambda}||(n-1),\beta J_f\rangle. \quad (67)$$

The other term (65) describes a scattering transition between states with the same number of phonons and is determined by the quasiparticle matrix elements

$$\mathcal{M}^{(-)}_{rs}(\lambda) = \langle r||\mathcal{M}_\lambda||s\rangle[u_r v_s - (-)^\lambda u_s v_r] \quad (68)$$

multiplied by the density matrix

$$\rho_{\alpha\beta}([r\times s]^\lambda) = \langle n,\beta||(\alpha^\dagger_r\times\beta_s)^\lambda||n,\alpha\rangle \quad (69)$$

given by Eq. (47).

IV. APPLICATION TO ^{20}O

For illustrative purposes, we compute the low-lying spectrum and the dipole strength distribution of the neutron-rich ^{20}O.

As anticipated in the Introduction, we make use of the nucleon-nucleon optimized chiral potential $V_\chi = \mathrm{NNLO_{opt}}$ determined by fixing the coupling constants at next-to-next-to-leading order through a new optimization method in the analysis of the phase shifts, which minimizes the effects of the three-nucleon force [57]. Though reproducing several bulk and spectroscopic properties of light and medium-light nuclei, this potential overestimates the binding energy in medium and heavy nuclei. In our previous works on heavy nuclei, we added a phenomenological, density-dependent potential derived from a contact three-body interaction [59,60] which counteracts the too-attractive character of $V_\chi = \mathrm{NNLO_{opt}}$ and yields more compressed and realistic HF spectra [58,61] and charge densities [41]. Dealing here with light nuclei, we use only V_χ.

The canonical HFB basis is generated in a configuration space which includes 11 harmonic oscillator major shells up to the principal quantum number $N_{\max} = 10$. This space is sufficient for reaching a good convergence of the single-particle spectra below and around the Fermi surface. In going, for instance, from $N_{\max} = 8$ to $N_{\max} = 10$, step by step, the energies change at most by $\sim$0.1 MeV at each step. More appreciable variations with $N_{\max}$ and the harmonic oscillator frequency occur in the spectrum far above the Fermi surface, a general feature of HF and HFB. We have put $\hbar\omega_{\mathrm{HO}} = 16$ MeV, which is close to the empirical value.

The energy of the HFB vacuum is $E_{\mathrm{HFB}} = -51.67$ MeV, corresponding to a binding energy per nucleon $B_{\mathrm{HF}}/A \simeq 2.58$ MeV three times smaller than the experimental value $B_{\mathrm{exp}}/A = 7.57$ MeV. This is consistent with a HF calculation performed for closed-shell nuclei using a UCOM interaction derived from an Argonne potential [62], which underestimates the binding energies by a factor two.

The TDA phonons are determined in a space which includes up to the (pfh) major shell. Their energy and structure remain practically unchanged if the two-quasiparticle space is further enlarged. They are free of spurious admixtures by virtue of the Gramm-Schmidt orthogonalization of the two-quasiparticle states to the c.m. and the particle-number states.

The correlated two-phonon states $|\alpha_2\rangle$ (40) are generated in a space truncated according to the energy $E_{\lambda_1} + E_{\lambda_2}$ of the basis states $|(\lambda_1\times\lambda_2)^\beta\rangle \equiv \{O^\dagger_{\lambda_1}\times|\lambda_2\rangle\}^\beta$. They are added to the HFB vacuum plus the TDA one-phonon basis to solve the full eigenvalue equations (53) determining the ground and excited EMPM states of the form (60).

The ground-state correlation energy depends critically on the truncation of the two-phonon space. It goes from $E_{\mathrm{corr}} \simeq -4.1$ MeV in correspondence of a 30-MeV cutoff to $E_{\mathrm{corr}} = -18.05$ MeV if we use the full two-phonon basis allowed by the number of shells up to the (pfh) shell. When added to the HFB energy, it yields a binding energy per nucleon $B_{\mathrm{th}}/A \simeq 3.49$ MeV. The correlation energy is expected to increase substantially in absolute value if we include all two-phonon states composed of all TDA phonons allowed by the dimensions of the HO space.

This can be inferred from an ongoing systematic study of the two-phonon correlation energy in closed-shell nuclei to be submitted for publication in the near future. An EMPM calculation, using the same $\mathrm{NNLO_{opt}}$ potential adopted here and performed in HO spaces of variable dimensions, yields for the HF and the two-phonon correlation energies of ^{16}O $E_{\mathrm{HF}} \sim -51$ MeV and $E_{\mathrm{corr}} \sim -58$ MeV, respectively. These values do not change in going from $N_{\max} = 8$ to $N_{\max} = 14$, as long as all two-phonon states allowed by $N_{\max}$ are included.

Even when all two-phonon states are included, the corresponding binding energy per nucleon, $B_{\mathrm{th}}/A \sim 6.8$ MeV, approaches but does not reach the experimental value $B_{\mathrm{exp}}/A = 7.98$ MeV. More complex configurations, chiefly four-phonon states, are needed. This is suggested also by

CC-theory calculations which take effectively into account (4p-4h) configurations and reproduce the ground-state energies [3].

Unlike the ground state, the one-phonon excited states are insensitive to the dimensions of the two-phonon space. As the two-phonon energy cutoff raises from 30 to 60 MeV, the first excited 0^+ level gets shifted from $\simeq -1.6$ to $\simeq -1.7$ MeV with respect to the HFB vacuum. The ground-state energy, instead, is pushed from $\simeq -4.1$ MeV down to $\simeq -12.0$ MeV, thereby creating an unrealistic large gap between excited- and ground-state levels.

It would be necessary to include the three-phonon states in a space large enough to restore the correct separation between excited- and ground-state energies. These configurations are known to couple strongly to the one-phonon states and to push them down in energy [39].

Though feasible, in principle, the inclusion of a large number of three-phonon states would require unbearably lengthy calculations unless we resort to some efficient approximations. We plan to do this in the near future. We confine our illustrative calculation to the two-phonon space and consider the space truncation energy cutoff as a parameter to be fixed so as to reproduce roughly the first excited 1^- level. This is achieved by including two-phonon states composed of all TDA phonons, of both parities, fulfilling the condition $E_{\lambda_1} + E_{\lambda_2} \leqslant 30$ MeV.

One of our main goals is to compute the reduced transition strength,

$$B_\nu(E\lambda) = |\langle \nu||\mathcal{M}(E\lambda)||0^+\rangle|^2, \tag{70}$$

for the electric multipole operator

$$\mathcal{M}(E\lambda\mu) = \sum_{i=1}^{Z} e_i r_i^\lambda Y_{\lambda\mu}(\hat{r}_i). \tag{71}$$

The transition amplitudes are obtained by inserting the wave functions (60) up to two phonons into the formula (62) and making use of Eqs. (63)–(65). We get

$$\begin{aligned}\langle \nu||\mathcal{M}(E\lambda)||0_1^+\rangle &= \mathcal{C}_0^{(0_1^+)} \sum_{\beta_1} \mathcal{C}_{\beta_1}^{(\nu)} \langle \beta_1||\mathcal{M}(\lambda)||0\rangle \\ &+ (-)^\lambda \sum_{\beta_1\alpha_2} \mathcal{C}_{\alpha_2}^{(0_1^+)} \mathcal{C}_{\beta_1}^{(\nu)} \mathcal{M}_{\beta_1\alpha_2}(\lambda) \\ &+ \sum_{\alpha_2\beta_2} \mathcal{C}_{\alpha_2}^{(0^+)} \mathcal{C}_{\beta_2}^{(\nu)} \langle \beta_2||\mathcal{M}(\lambda)||\alpha_2\rangle, \end{aligned} \tag{72}$$

where

$$\mathcal{M}_{\beta_1\alpha_2}(\lambda) = [\lambda]^{-1/2} \sum_x \langle x\lambda||\mathcal{M}(\lambda)||0\rangle X^{\alpha_2}_{(x\lambda)(\beta_1\lambda)} \tag{73}$$

and $X^{(\alpha_2)}_{(x\lambda)(\beta_1\lambda)} = \langle \alpha_2, 0^+||O^\dagger_{x\lambda}||\beta_1\lambda\rangle$.

The first term couples the HFB vacuum to the TDA one-phonon states and is dominant, in general. The second contributes if the ground state has sizable two-phonon components, while the third may be non-negligible only if both ground and excited states have appreciable two-phonon components. Because it is not the case here, this latter term has been neglected because its computation is too time consuming.

For $\lambda = 1$ it is necessary to check if and to what extent we dispose of the spurious c.m. admixtures within the EMPM. We see from Eq. (72) that the first term is entirely determined by the TDA transition amplitude, which is free of spurious components. We have checked, in fact, that the contribution of the isoscalar dipole operator to this term is zero. Equation (73) shows that the TDA transition amplitude determines also the smaller second term. Because the constituent TDA phonons are free of spurious admixtures, this piece may get spurious contributions only from the exchange terms of the overlap matrix $\mathcal{D}$ (49) entering the amplitude X [Eq. (48)]. The exchange terms of $\mathcal{D}$, present in the density matrix ρ [Eq. (47)], may contaminate also the third term, which we have neglected. In our case, because of the spurious admixtures present in the second term, the isoscalar transition strengths are of the order $\sim 10^{-4}\ e^2\,\mathrm{fm}^2$, at most. These small, unwanted, contributions are removed by using, as common practice, the intrinsic $E1$ operator

$$\mathcal{M}(E1\mu) = \frac{N}{A} \sum_{i=1}^{Z} e_i r_i Y_{1\mu}(\hat{r}_i) - \frac{Z}{A} \sum_{i=1}^{N} e_i r_i Y_{1\mu}(\hat{r}_i). \tag{74}$$

Once the $E1$ reduced strength is evaluated, we compute the cross section

$$\sigma = \int_0^\infty \sigma(\omega) d\omega = \frac{16\pi^3}{9\hbar c} \int_0^\infty \omega \mathcal{S}(E1,\omega) d\omega, \tag{75}$$

where $\mathcal{S}(E1,\omega)$ is the strength function

$$\begin{aligned}\mathcal{S}(E1,\omega) &= \sum_\nu B_\nu(E1)\, \delta(\omega - \omega_\nu) \\ &\approx \sum_\nu B_\nu(E1)\, \rho_\Delta(\omega - \omega_\nu). \end{aligned} \tag{76}$$

Here ω is the energy variable, ω_ν the energy of the transition from the ground to the ν_{th} excited state of spin $J^\pi = 1^-$, and

$$\rho_\Delta(\omega - \omega_\nu) = \frac{\Delta}{2\pi} \frac{1}{(\omega - \omega_\nu)^2 + \left(\frac{\Delta}{2}\right)^2} \tag{77}$$

is a Lorentzian of width Δ, which replaces the δ function as a weight of the reduced strength.

After integration, the cross section becomes

$$\sigma = \frac{16\pi^3}{9\hbar c} m_1, \tag{78}$$

where

$$m_1(E1) = \sum_\nu \omega_\nu B_\nu(E1) \tag{79}$$

is the first moment.

If the Hamiltonian does not contain momentum-dependent and exchange terms, m_1 fulfills the classical energy weighted Thomas-Reiche-Kuhn (TRK) sum rule

$$m_1(E1) = \frac{\hbar^2}{2m} \frac{9}{4\pi} \frac{NZ}{A} e^2 \tag{80}$$

and the total cross section assumes the value

$$\sigma(E1) = (2\pi)^2 \frac{\hbar^2}{2m} \frac{e^2}{\hbar c} \frac{NZ}{A} = 60 \frac{NZ}{A} (\text{MeVmb}). \tag{81}$$

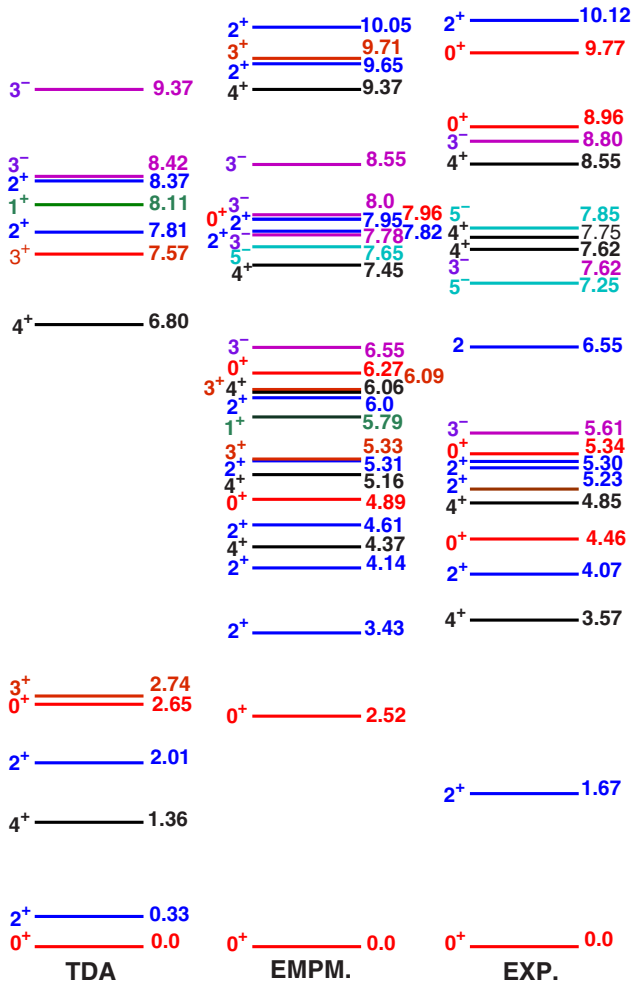

FIG. 1. Theoretical versus experimental level scheme of ^{20}O.

TABLE I. Weight of the n-phonon components in the ground and some low-lying states.

State	W_0	W_1	W_2
0_1^+	0.86	0.01	0.13
0_2^+	0.01	0.02	0.97
0_3^+	0.00	0.37	0.63
0_4^+	0.00	0.54	0.46
2_1^+	0.00	0.88	0.12
2_2^+	0.00	0.08	0.92
2_3^+	0.00	0.31	0.69
2_4^+	0.00	0.54	0.46
4_1^+	0.00	0.89	0.11
4_2^+	0.00	0.04	0.96
1_1^-	0.00	0.09	0.91
1_2^-	0.00	0.22	0.78
1_3^-	0.00	0.14	0.86
1_4^-	0.00	0.22	0.78
3_1^-	0.00	0.16	0.84
3_2^-	0.00	0.18	0.82

A. Energy levels

The TDA and EMPM level schemes are compared to the experimental spectrum [43–46] in Fig. 1.

It is worth stressing that the EMPM levels are referred to the energy of the correlated ground state. Because this is shifted downward with respect to the HFB vacuum by the coupling to the two-phonon states, the dominantly one-phonon energy levels, less affected by the phonon coupling, appear at higher energies than the corresponding TDA levels, which are referred to the HFB vacuum.

The opposite occurs in extended (Q)RPA, where the levels are shifted downward with respect to (Q)RPA. This contradiction is easily explained. The (Q)RPA extensions take into account only the coupling between (Q)RPA phonons and two-phonon configurations, responsible for the downward shift of the levels, and ignore the zero-phonon to two-phonon coupling.

The crucial role played by the two-phonon states emerges clearly from the plot. The TDA spectrum is far from resembling the experimental one. Once the two phonons are included, the calculation yields a sequence of levels of the same density of the experimental scheme. There is an almost one-to-one correspondence between theoretical and experimental levels.

However, serious discrepancies, especially concerning the 0_2^+ and 2_1^+ first excited levels, occur. The 0_2^+ is ∼2 MeV below the measured level, while the 2_1^+ is ∼2.4 MeV above. This energy inversion is in contrast also with TDA whose first 2_1^+ is below the 0_2^+. The TDA 2_1^+ level is actually almost degenerate with the HFB ground state. In general, all first excited TDA levels are too low in energy, suggesting that the pairing component of the chiral potential might be too weak. Indeed, if the strength of the neutron pairing field (14) is multiplied by a factor 1.7, the TDA 0_2^+ and 2_1^+ energies raise, respectively, to $E_{0^+} = 3.88$ MeV and $E_{2^+} = 1.46$ MeV, close to the corresponding experimental levels.

Only the decay rate of the first 2_1^+ was measured [43]. The calculation yields $B(E2; 0_1^+ \to 2_1^+) \simeq 0.2\ e^2\,\mathrm{fm}^4$, two orders of magnitude smaller than the experimental value, $B(E2; 0_1^+ \to 2_1^+) \simeq 29\ e^2\,\mathrm{fm}^4$.

The key for understanding the reason of such a failure is in the phonon composition of the low-lying states. Unlike the other first excited states, mainly of two-phonon nature, 2_1^+ and 4_1^+ are predominantly one-phonon states (Table I). The TDA phonon with largest weight in the 2_1^+ is the lowest in energy and is composed mainly of neutron two-quasiparticle configurations belonging to the (s,d) shell (Table II), which obviously do not contribute to the transition. This neutron dominance persists even if we enlarge the two-phonon space so as to include all two-phonon states of energies $E_{\lambda_1} + E_{\lambda_2} \leqslant 50$ MeV.

It is clearly necessary to enhance the amplitudes of the proton p-h core components of the TDA phonons over the neutron two-quasiparticles. This can be done by including the three-phonon states, which are known to couple strongly to TDA phonons in ^{16}O [39]. A complementary recipe may consist of improving the HFB quasiparticle spectrum, which amounts to improving the nuclear potential.

TABLE II. Two-quasiparticle composition of the first 2^+ TDA phonon.

$r_\pi s_\pi$	c^π_{rs}	$r_\nu s_\nu$	c^ν_{rs}
$0d_{5/2}0s_{1/2}$	−0.019	$0d_{5/2}0d_{5/2}$	0.874
$0d_{3/2}0s_{1/2}$	−0.021	$0d_{5/2}0s_{1/2}$	−0.459
$0f_{7/2}0p_{3/2}$	−0.023	$0d_{3/2}0s_{1/2}$	−0.013
$0f_{5/2}0p_{3/2}$	−0.010	$0d_{5/2}0d_{3/2}$	−0.098
$0f_{5/2}0p_{1/2}$	0.030	$1s_{1/2}0d_{3/2}$	0.074
$1d_{3/2}0s_{1/2}$	0.015	$0d_{5/2}0d_{3/2}$	0.035
$1f_{7/2}0p_{3/2}$	−0.017	$1p_{3/2}0p_{3/2}$	−0.010
$1f_{5/2}0p_{3/2}$	0.014	$0f_{7/2}0p_{3/2}$	0.017
		$0d_{5/2}1d_{5/2}$	0.015
		$0d_{5/2}2s_{1/2}$	−0.023
		$0d_{3/2}2s_{1/2}$	−0.014
		$0f_{5/2}0p_{1/2}$	0.014
		$1d_{3/2}0s_{1/2}$	0.011
		$0d_{5/2}1d_{3/2}$	0.026
		$1s_{1/2}1d_{3/2}$	−0.012
		$0d_{3/2}1d_{3/2}$	0.015
		$0d_{5/2}0g_{9/2}$	0.022
		$0d_{3/2}0g_{7/2}$	0.013
		$1f_{7/2}0p_{3/2}$	0.013
		$1f_{5/2}0p_{3/2}$	−0.011
		$1f_{5/2}0p_{1/2}$	−0.017

B. Dipole response

From comparing the EMPM versus the TDA spectra in Fig. 2 one infers that the phonon coupling induces a severe fragmentation of the strength and a consequent quenching of the single peaks.

Of special interest is the splitting of the low-lying TDA peak into several smaller peaks with the appearance of two levels below the neutron decay threshold, in agreement with the data obtained in a virtual-photon scattering experiment [26,27] at around 100 MeV/nucleon. As shown in Fig. 3, the strengths of these two levels are within the experimental uncertainties of the measured values. It may be worth reminding ourselves that these strengths are underestimated by an order of magnitude in phenomenological shell-model calculations [27].

Two levels are produced just around the (γ,n) threshold. They get manifest (Fig. 4) as a very small hump in the cross section, which, in turn, corresponds to the hump in the 7–8-MeV energy interval of the measured cross section [25].

All these four low-lying 1^- states have a dominant two-phonon character (Table I). Their one-phonon components are predominantly linear combinations of two-quasiparticle configurations describing excitations of the valence neutrons from the (sd) to the (pf) shells. By virtue of this overwhelming neutron dominance, illustrated for the lowest 1^- of energy $\omega = 8.397$ MeV on Table III, these TDA states can be

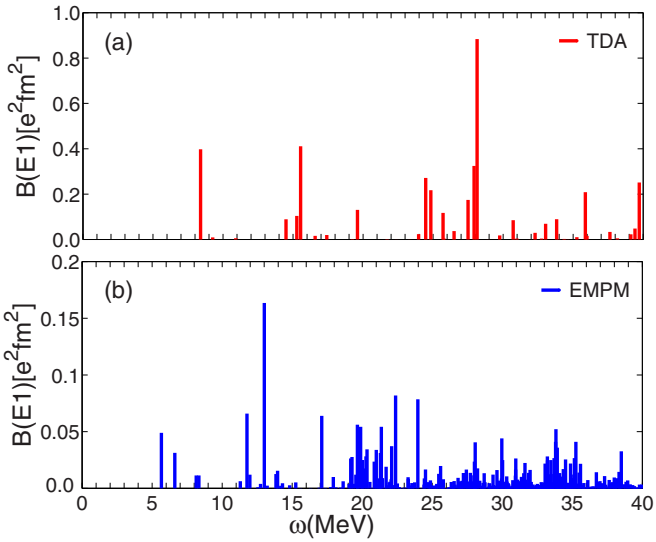

FIG. 2. TDA (a) and EMPM (b) $E1$ strength distribution in ^{20}O.

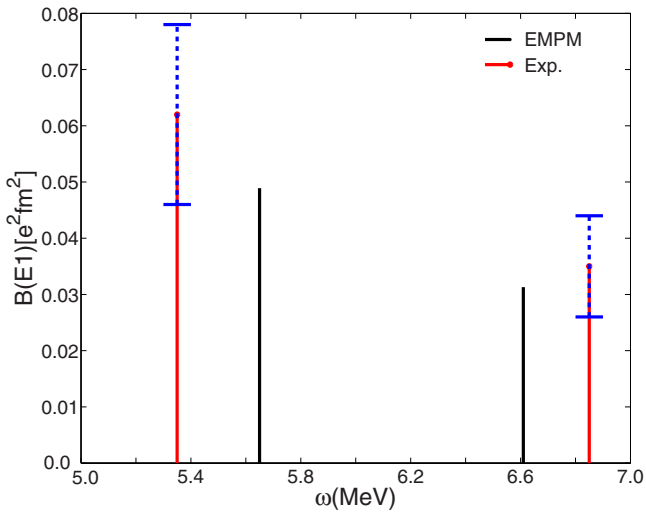

FIG. 3. Theoretical versus experimental [27] $E1$ reduced strengths of the two lowest levels in ^{20}O.

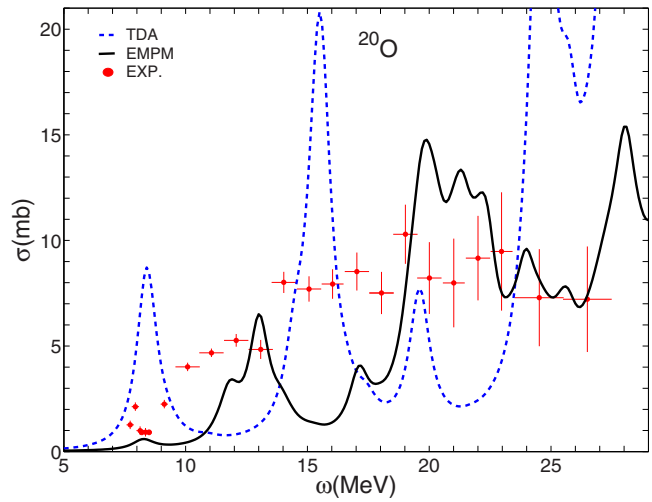

FIG. 4. Theoretical versus experimental $E1$ cross section in ^{20}O. The contribution of the lowest two levels in the interval 5–7 MeV, measured in Ref. [27], is not included to make a consistent comparison with the data of Ref. [25]. We have used a Lorentz width $\Delta = 1$ MeV.

TABLE III. Proton (π) and neutron (ν) two-quasiparticle composition of two 1^- TDA phonons.

$r_\pi s_\pi$	c^π_{rs}	$r_\nu s_\nu$	c^ν_{rs}
	$\omega = 8.397$ MeV		
$0d_{5/2}0p_{3/2}$	−0.188	$0d_{5/2}0p_{3/2}$	−0.174
$0d_{3/2}0p_{3/2}$	−0.053	$1s_{1/2}0p_{3/2}$	0.102
$0d_{3/2}0p_{1/2}$	0.117	$0d_{3/2}0p_{1/2}$	0.117
$1d_{3/2}0p_{1/2}$	−0.063	$0d_{5/2}1p_{3/2}$	0.718
		$1s_{1/2}1p_{3/2}$	−0.505
		$0d_{3/2}1p_{3/2}$	0.064
		$1s_{1/2}1p_{1/2}$	0.192
		$0d_{3/2}1p_{1/2}$	0.119
		$0d_{5/2}0f_{7/2}$	0.160
		$0d_{5/2}0f_{5/2}$	−0.051
		$0d_{3/2}0f_{5/2}$	−0.051
		$1d_{3/2}1p_{1/2}$	0.064
		$0d_{5/2}1f_{7/2}$	0.075
	$\omega = 28.143$ MeV		
$0d_{5/2}0p_{3/2}$	0.417	$0d_{5/2}0p_{3/2}$	−0.318
$1s_{1/2}0p_{3/2}$	−0.022	$1s_{1/2}0p_{3/2}$	−0.112
$1s_{1/2}0p_{1/2}$	0.055	$1s_{1/2}0p_{1/2}$	−0.043
$0d_{3/2}0p_{3/2}$	0.120	$0d_{3/2}0p_{3/2}$	−0.065
$0d_{3/2}0p_{1/2}$	−0.169	$0d_{3/2}0p_{1/2}$	−0.071
$1d_{5/2}0p_{3/2}$	0.072	$0d_{5/2}1p_{3/2}$	−0.015
$2s_{1/2}0p_{1/2}$	0.108	$0d_{5/2}0f_{7/2}$	0.060
$1d_{3/2}0p_{3/2}$	−0.024	$1d_{5/2}0p_{3/2}$	0.110
$1d_{3/2}0p_{1/2}$	−0.086	$1d_{5/2}1p_{3/2}$	0.027
		$1d_{5/2}0f_{7/2}$	−0.090
		$2s_{1/2}1p_{3/2}$	−0.024
		$2s_{1/2}0p_{1/2}$	0.159
		$2s_{1/2}1p_{1/2}$	−0.031
		$0d_{3/2}0f_{5/2}$	−0.049
		$1d_{3/2}0p_{1/2}$	−0.049
		$1d_{3/2}1p_{3/2}$	−0.020
		$1d_{3/2}0f_{5/2}$	−0.051
		$0d_{5/2}1f_{7/2}$	0.595
		$0d_{5/2}2p_{3/2}$	−0.217
		$1s_{1/2}2p_{3/2}$	−0.392

associated with the PDR. However, they represent a small fraction of the total wave functions, as Table I clearly shows.

Quite different is the structure of the high-energy TDA phonons, falling in the region of the GDR. An example is given in Table III. The phonon of energy $\omega = 28.143$ MeV contains proton and neutron p-h components in opposition of phase, in addition to neutron particle-particle excitations, consistently with the picture underlying the GDR.

The calculation reproduces only qualitatively the trend of the experimental cross section. This is underestimated in the regions 8–12 and 14–18 MeV. The strength collected by all the states up to ∼15 MeV accounts only for ∼6% of the TRK sum rule, just half the ∼12% fraction estimated experimentally [25,47]. The cross section integrated up to ∼27 MeV accounts for ∼38% of the TRK sum rule to be compared with the ∼45% determined experimentally.

Most 1^- states have sizable, or even dominant, two-phonon components. There is a reason for that. Many of them are obtained by coupling $\sim 1\hbar\omega$ phonons with $0\hbar\omega$ two-quasiparticle states and, therefore, are almost degenerate with the $\sim 1\hbar\omega$ 1^- single phonons.

The three-phonon configurations are expected to reduce the weight of the two phonons in favor of the one-phonon states. In particular, they should increase the amplitudes of p-h core components, with consequent enhancement of the transition strengths from the ground state.

V. CONCLUSIONS

The formalism of the EMPM has been shown to remain unchanged in going from the p-h to the quasiparticle scheme. Also in this new context, the method does not rely on approximations except for the one inherent in the HFB transformation. Even this limitation is minimized. In fact, by virtue of the phonon structure of the states, the spurious admixtures, induced by the particle number violation and the c.m. motion, are eliminated to a large extent by a Gram-Schmidt orthogonalization procedure.

The correlated basis incorporates high-energy configurations even if the calculation is performed in a truncated space. However, including basis states with an increasing number of phonons implies lengthier and lengthier calculations which eventually render the task practically impossible. We have, therefore, to rely on a fast convergence with the phonon number.

In the application to the neutron-rich ^{20}O, the calculation was performed in a truncated two-phonon space. The space truncation was dictated by the necessity of getting a realistic separation between the excited- and ground-state energies. A calculation using the full two-phonon basis, while affecting little the excited states, would have depressed strongly the ground state. Only the three phonons, which couple strongly to the one-phonon states and push them down in energy, can reduce drastically such a gap.

The coupling to three phonons is also expected to enhance the weight of the one-phonon over the two-phonon states and, in particular, should increment the amplitude of the core components, thereby promoting an enhancement of transition strengths, including the $E2$ decay strength of the first 2^+ state. Were not this the case, it would be necessary to improve the HFB basis by upgrading the optimized chiral potential.

Including a substantial number of three-phonon states requires unbearably lengthy calculations, unless we resort to approximations. One may consist of neglecting the interaction among phonons within the $n = 3$ subspace described by the matrix elements $\mathcal{V}^\sigma_{\lambda\alpha\lambda'\alpha'}$ in Eq. (45) and, then, extracting a basis of linear independent states from the unperturbed set $|(\lambda \times \alpha)^\beta\rangle$ by the Choleski decomposition method. We are testing this approximation on the doubly magic ^{16}O for the p-h scheme.

Although confined within a truncated space, the two-phonon states came out to play a crucial role. They are responsible for the strong fragmentation of the dipole strength, in qualitative agreement with the data, and for generating a scheme of levels which are almost in one-to-one correspondence with the experimental energies. These

important effects remain even in a larger two-phonon space and can be only amplified by the inclusion of three phonons.

ACKNOWLEDGMENTS

This work was partly supported by the Czech Science Foundation (P203-13-07117S). Two of the authors (F.K. and P.V.) thank the Istituto Nazionale di Fisica Nucleare (Italy) for financial support. Highly appreciated was the access to computing and storage facilities provided by the Meta Centrum under Program No. LM2010005 and the CERIT-SC under the program Centre CERIT Scientific Cloud, part of the Operational Program Research and Development for Innovations, Register No. CZ.1.05/3.2.00/08.0144.

[1] B. R. Barrett, P. Navrátil, and J. P. Vary, Ab initio no core shell model, Prog. Part. Nucl. Phys. **69**, 131 (2013).
[2] D. J. Dean and M. Hjorth-Jensen, Coupled-cluster approach to nuclear physics, Phys. Rev. C **69**, 054320 (2004).
[3] G. Hagen, T. Papenbrock, M. Hjorth-Jensen, and D. J. Dean, Coupled-cluster computations of atomic nuclei, Rep. Prog. Phys. **77**, 096302 (2014).
[4] E. Caurier, G. Martínez-Pinedo, F. Nowacki, A. Poves, and A. P. Zuker, The shell model as a unified view of nuclear structure, Rev. Mod. Phys. **77**, 427 (2005).
[5] T. Otsuka, M. Honma, N. Shimizu, and Y. Utsuno, Monte-Carlo shell model for atomic nuclei, Prog. Part. Nucl. Phys. **47**, 319 (2001).
[6] N. Shimizu, T. Otsuka, T. Mizusaki, and M. Honma, Monte-Carlo shell model calculations of Xe and Ba isotopes, J. Phys.: Conf. Ser. **49**, 178 (2006).
[7] K. Sieja, G. Martínez-Pinedo, L. Coquard, and N. Pietralla, Description of proton-neutron mixed-symmetry states near ^{132}Sn within a realistic large scale shell model, Phys. Rev. C **80**, 054311 (2009).
[8] D. Bianco, F. Andreozzi, N. Lo Iudice, A. Porrino, and F. Knapp, Matrix diagonalization algorithm and its applicability to the nuclear shell model, Phys. Rev. C **84**, 024310 (2011).
[9] D. Bianco, F. Andreozzi, N. Lo Iudice, A. Porrino, and F. Knapp, Importance-sampling diagonalization algorithm for large-scale shell model calculations on $N = 80$ isotones, Phys. Rev. C **85**, 034332 (2012).
[10] D. Bianco, N. Lo Iudice, F. Andreozzi, A. Porrino, and F. Knapp, Mixed-symmetry states in Te isotopes within a large-scale shell model approach, Phys. Rev. C **86**, 044325 (2012).
[11] D. Bianco, N. Lo Iudice, F. Andreozzi, A. Porrino, and F. Knapp, Spectroscopy of neutron-rich te and xe isotopes within a new shell model context, Phys. Rev. C **88**, 024303 (2013).
[12] M. Bender, P. H. Heenen, and P. G. Reinhard, Self-consistent mean-field models for nuclear structure, Rev. Mod. Phys. **75**, 121 (2003).
[13] G. F. Bertsch, P. F. Bortignon, and R. A. Broglia, Damping of nuclear excitations, Rev. Mod. Phys. **55**, 287 (1983).
[14] V. G. Soloviev, *Theory of Atomic Nuclei Quasiparticles and Phonons* (Institute of Physics Publishing, Bristol, Avon, UK, 1992).
[15] E. Litvinova, P. Ring, and V. Tselyaev, Relativistic quasiparticle time blocking approximation: Dipole response of open-shell nuclei, Phys. Rev. C **78**, 014312 (2008).
[16] E. Litvinova, P. Ring, V. Tselyaev, and K. Langanke, Relativistic quasiparticle time blocking approximation. II. Pygmy dipole resonance in neutron-rich nuclei, Phys. Rev. C **79**, 054312 (2009).
[17] P. Papakonstantinou and R. Roth, Large-scale second random-phase approximation calculations with finite-range interactions, Phys Rev. C **81**, 024317 (2010).
[18] D. Gambacurta, M. Grasso, and F. Catara, Collective nuclear excitations with skyrme-second random-phase approximation, Phys. Rev. C **81**, 054312 (2010).
[19] G. Colò and P. F. Bortignon, QRPA plus phonon coupling model and the photoabsorption cross section for ^{18,20,22}O, Nucl. Phys. A **696**, 427 (2001).
[20] N. Paar, D. Vretenar, E. Khan, and G. Colò, Exotic modes of excitation in atomic nuclei far from stability, Rep. Prog. Phys. **70**, 691 (2007).
[21] E. Litvinova, P. Ring, and V. Tselyaev, Mode Coupling and the Pygmy Dipole Resonance in a Relativistic Two-Phonon Model, Phys. Rev. Lett. **105**, 022502 (2010).
[22] N. Tsoneva, H. Lenske, and C. Stoyanov, Probing the nuclear neutron skin by low-energy dipole modes, Phys. Lett. B **586**, 213 (2004).
[23] N. Tsoneva and H. Lenske, Pygmy dipole resonances in the tin region, Phys. Rev. C **77**, 024321 (2008).
[24] R. Mohan, M. Danos, and L. C. Biedenharn, Three-fluid hydrodynamical model of nuclei, Phys. Rev. C **3**, 1740 (1971).
[25] A. Leistenschneider *et al.*, Photoneutron Cross Sections for Unstable Neutron-Rich Oxygen Isotopes, Phys. Rev. Lett. **86**, 5442 (2001).
[26] E. Tryggestad, T. Aumann, T. Baumann, D. Bazin, J. R. Beene, Y. Blumenfeld, B. A. Brown, M. Chartier, M. L. Halbert, P. Heckman, J. F. Liang, D. C. Radford, D. Shapira, M. Thoennessen, and R. L. Varner, Low-lying dipole strength in ^{20}O, Phys. Lett. B **541**, 52 (2002).
[27] E. Tryggestad, T. Baumann, P. Heckman, M. Thoennessen, T. Aumann, D. Bazin, Y. Blumenfeld, J. R. Beenec, T. A. Lewis, D. C. Radford, D. Shapira, R. L. Varner, B. A. Brown, M. Chartier, M. L. Halbert, and J. F. Liang, Low-lying $E1$ strength in ^{20}O, Phys. Rev. C **67**, 064309 (2003).
[28] N. Ryezayeva, T. Hartmann, Y. Kalmykov, H. Lenske, P. von Neumann-Cosel, V. Yu. Ponomarev, A. Richter, A. Shevchenko, S. Volz, and J. Wambach, Nature of Low-Energy Dipole Strength in Nuclei: The Case of a Resonance at Particle Threshold in ^{208}Pb, Phys. Rev. Lett. **89**, 272502 (2002).
[29] P. Adrich, A. Klimkiewicz, M. Fallot, K. Boretzky, T. Aumann, D. Cortina-Gil, U. Datta Pramanik, T. W. Elze, H. Emling, H. Geissel, M. Hellström, K. L. Jones, J. V. Kratz, R. Kulessa, Y. Leifels, C. Nociforo, R. Palit, H. Simon, G. Surówka, K. Sümmerer, and W. Waluś (LAND-FRS Collaboration), Evidence for Pygmy and Giant Dipole Resonances in ^{130}Sn and ^{132}Sn, Phys. Rev. Lett. **95**, 132501 (2005).
[30] A. Klimkiewicz, N. Paar, P. Adrich, M. Fallot, K. Boretzky, T. Aumann, D. Cortina-Gil, U. Datta Pramanik, T. W. Elze, H.

Emling, H. Geissel, M. Hellström, K. L. Jones, J. V. Kratz, R. Kulessa, C. Nociforo, R. Palit, H. Simon, G. Surówka, K. Sümmerer, D. Vretenar, and W. Waluś (LAND Collaboration), Nuclear symmetry energy and neutron skins derived from pygmy dipole resonances, Phys. Rev. C **76**, 051603 (2007).

[31] R. Schwengner, G. Rusev, N. Benouaret, R. Beyer, M. Erhard, E. Grosse, A. R. Junghans, J. Klug, K. Kosev, L. Kostov, C. Nair, N. Nankov, K. D. Schilling, and A. Wagner, Dipole response of ^{88}Sr up to the neutron-separation energy, Phys. Rev. C **76**, 034321 (2007).

[32] D. Savran, M. Babilon, A. M. van den Berg, M. N. Harakeh, J. Hasper, A. Matic, H. J. Wörtche, and A. Zilges, Nature of the Pygmy Dipole Resonance in ^{140}Ce studied in $(\alpha,\alpha'\gamma)$ Experiments, Phys. Rev. Lett. **97**, 172502 (2006).

[33] A. Tamii *et al.*, Complete Electric Dipole Response and the Neutron Skin in ^{208}Pb, Phys. Rev. Lett. **107**, 062502 (2011).

[34] I. Poltoratska *et al.*, Pygmy dipole resonance in ^{208}Pb, Phys. Rev. C **85**, 041304 (2012).

[35] D. Savran, T. Aumann, and A. Zilges, Experimental studies of the pygmy dipole resonance, Prog. Part. Nucl. Phys. **70**, 210 (2013).

[36] N. Paar, The quest for novel modes of excitation in exotic nuclei, J. Phys. G: Nucl. Part. Phys. **37**, 064014 (2010).

[37] F. Andreozzi, F. Knapp, N. Lo Iudice, A. Porrino, and J. Kvasil, Exact formulation and solution of the nuclear eigenvalue problem in a microscopic multiphonon space, Phys. Rev. C **75**, 044312 (2007).

[38] F. Andreozzi, F. Knapp, N. Lo Iudice, A. Porrino, and J. Kvasil, Multiphonon nuclear response in ^{16}O: A microscopic treatment equivalent to the shell model, Phys. Rev. C **78**, 054308 (2008).

[39] D. Bianco, F. Knapp, N. Lo Iudice, F. Andreozzi, and A. Porrino, Upgraded formulation of the nuclear eigenvalue problem in a microscopic multiphonon basis, Phys. Rev. C **85**, 014313 (2012).

[40] D. Bianco, F. Knapp, N. Lo Iudice, F. Andreozzi, A. Porrino, and P. Veselý, Electric dipole response in ^{208}Pb within a new microscopic multiphonon approach, Phys. Rev. C **86**, 044327 (2012).

[41] F. Knapp, N. Lo Iudice, P. Veselý, F. Andreozzi, G. De Gregorio, and A. Porrino, Dipole response in ^{208}Pb within a self-consistent multiphonon approach, Phys. Rev. C **92**, 054315 (2015).

[42] F. Knapp, N. Lo Iudice, P. Veselý, F. Andreozzi, G. De Gregorio, and A. Porrino, Dipole response in ^{132}Sn within a self-consistent multiphonon approach, Phys. Rev. C **90**, 014310 (2014).

[43] D. R. Tilley, C. M. Cheves, J. H. Kelley, S. Raman, and H. R. Weller, Energy levels of light nuclei, $A = 20$, Nucl. Phys. A **636**, 249 (1998).

[44] J. K. Jewell, L. A. Riley, P. D. Cottle, K. W. Kemper, T. Glasmacher, R. W. Ibbotson, H. Scheit, M. Chromik, Y. Blumenfeld, S. E. Hirzebruch, F. Maréchal, and T. Suomijärvi, Proton scattering on the radioactive nucleus ^{20}O and the $0^+_g s \rightarrow 2^+_1$ transition in the neutron-rich oxygen isotopes, Phys. Lett. B **454**, 181 (1999).

[45] E. Khan *et al.*, Low-lying collective states in neutron-rich oxygen isotopes via proton scattering, Phys. Lett. B **490**, 45 (2000).

[46] M. Stanoiu *et al.*, N=14 and 16 shell gaps in neutron-rich oxygen isotopes, Phys. Rev. C **69**, 034312 (2004).

[47] T. Aumann, Giant resonances in exotic nuclei experimental status and perspectives, Nucl. Phys. A **805**, 198c (2008).

[48] G. R. Jansen, J. Engel, G. Hagen, P. Navratil, and A. Signoracci, *Ab initio* Coupled-Cluster Effective Interactions for the Shell Model: Application to Neutron-Rich Oxygen and Carbon Isotopes, Phys. Rev. Lett. **113**, 142502 (2014).

[49] O. Jensen, G. Hagen, M. Hjorth-Jensen, B. A. Brown, and A. Gade, Quenching of Spectroscopic Factors for Proton Removal in Oxygen Isotopes, Phys. Rev. Lett. **107**, 032501 (2011).

[50] G. Hagen, M. Hjorth-Jensen, G. R. Jansen, R. Machleidt, and T. Papenbrock, Continuum Effects and Three-Nucleon Forces in Neutron-Rich Oxygen Isotopes, Phys. Rev. Lett. **108**, 242501 (2012).

[51] J. D. Holt, J. Menéndez, and A. Schwenk, Chiral three-nucleon forces and bound excited states in neutron-rich oxygen isotopes, Eur. Phys. J. A **49**, 39 (2013).

[52] E. Khan and N. V. Giai, Low-lying 2^+ states in neutron-rich oxygen isotopes in quasiparticle random phase approximation, Phys. Lett. B **472**, 253 (2000).

[53] H. Sagawa and T. Suzuki, Pigmy and giant dipole states in oxygen isotopes, Phys. Rev. C **59**, 3116 (1999).

[54] D. Vretenar, N. Paar, P. Ring, and G. A. Lalazissis, Collectivity of the low-lying dipole strength in relativistic random phase approximation, Nucl. Phys. A **692**, 496 (2001).

[55] M. Tohyama and A. S. Umar, Dipole resonances in oxygen isotopes in time-dependent density-matrix theory, Phys. Lett. B **516**, 415 (2001).

[56] M. Tohyama and A. S. Umar, Quadrupole resonances in unstable oxygen isotopes in time-dependent density-matrix formalism, Phys. Lett. B **549**, 72 (2002).

[57] A. Ekström, G. Baardsen, C. Forssén, G. Hagen, M. Hjorth-Jensen, G. R. Jansen, R. Machleidt, W. Nazarewicz, T. Papenbrock, J. Sarich, and S. M. Wild, Optimized Chiral Nucleon-Nucleon Interaction at Next-to-Next-to-Leading Order, Phys. Rev. Lett. **110**, 192502 (2013).

[58] D. Bianco, F. Knapp, N. Lo Iudice, P. Veselý, F. Andreozzi, G. De Gregorio, and A. Porrino, A self-consistent study of multipole response in neutron-rich nuclei using a modified realistic potential, J. Phys. G: Nucl. Part. Phys. **41**, 025109 (2014).

[59] M. Waroquier, K. Heyde, and H. Vincx, Antisymmetry in the three-nucleon-interaction matrix elements, Phys. Rev. C **13**, 1664 (1976).

[60] A. Günther, R. Roth, H. Hergert, and S. Reinhardt, Systematics of binding energies and radii based on realistic two-nucleon plus phenomenological three-nucleon interactions, Phys. Rev. C **82**, 024319 (2010).

[61] H. Hergert, P. Papakonstantinou, and R. Roth, Quasiparticle random-phase approximation with interactions from the similarity renormalization group, Phys. Rev. C **83**, 064317 (2011).

[62] R. Roth, N. Papakonstantinou, P. Paar, H. Hergert, T. Neff, and H. Feldmeier, Hartree-fock and many body perturbation theory with correlated realistic *NN* interactions, Phys. Rev. C **73**, 044312 (2006).